SUPPORTING INFORMATION

***In situ* growth of Metal-Organic Frameworks in Three-Dimensional Aligned Lumen Arrays of Wood for Rapid and Highly Efficient Organic Pollutants Removal**

Ruixue Guo[1]†, Xiaohui Cai[1]†, Hanwen Liu[1], Zi Yang[1], Yajie Meng [1], Fengjuan Chen[1*], Yiju Li[2*], Baodui Wang[1*]

[1] *State Key Laboratory of Applied Organic Chemistry and Key Laboratory of Nonferrous Metal Chemistry and Resources Utilization of Gansu Province, Lanzhou University Gansu, Lanzhou, 730000, P. R. China*
[2] *Department of Materials Science and Engineering, College of Engineering, Peking University, Beijing 100871, P. R. China*

*Email: chenfj@lzu.edu.cn; liyijuliyiju2014@outlook.com; wangbd@lzu.edu.cn

†These authors contribute equally to this work.

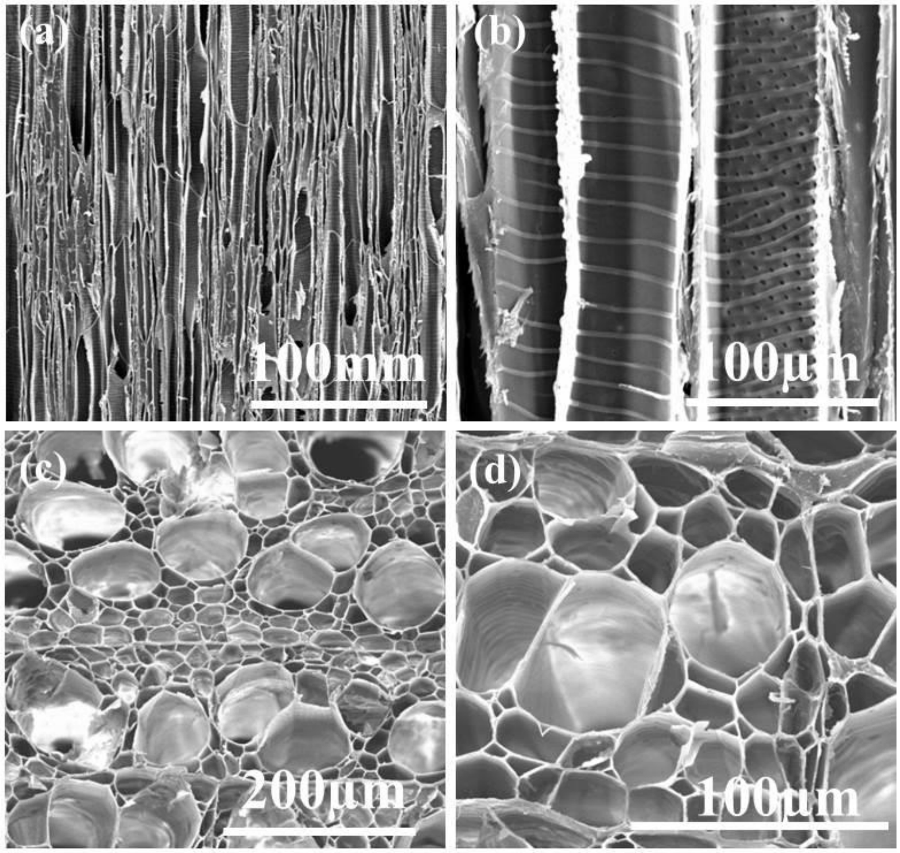

Figure S1. (a) SEM image of natural wood. There are numerous long and irregular microchannels in wood. (b) High resolution SEM image of wood channels. (c, d) SEM images showing the top view of the natural wood.

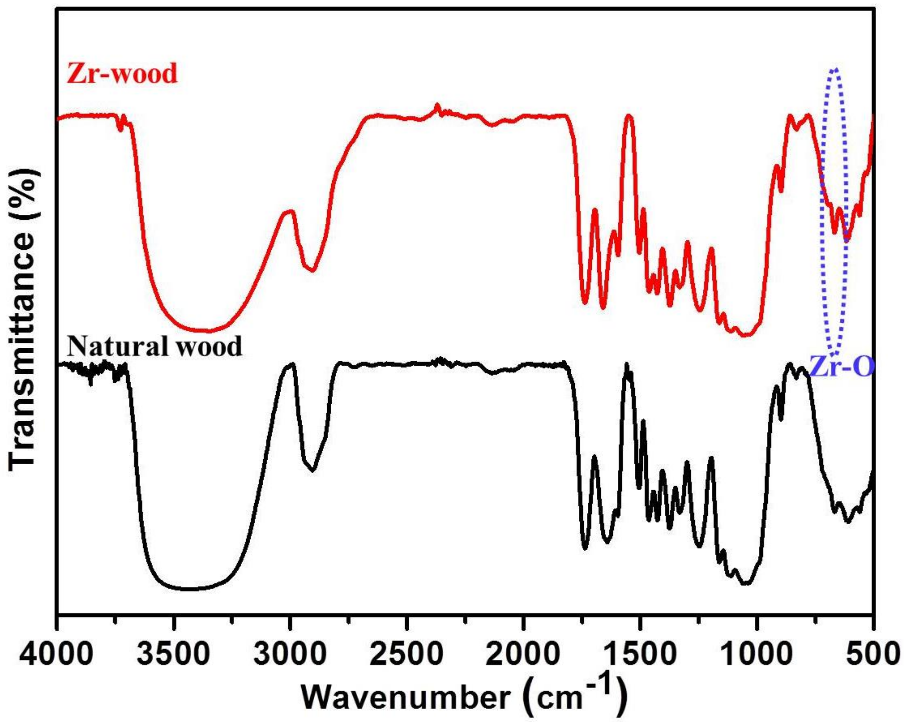

Figure S2. Infrared spectrum of the natural wood and Zr-wood.

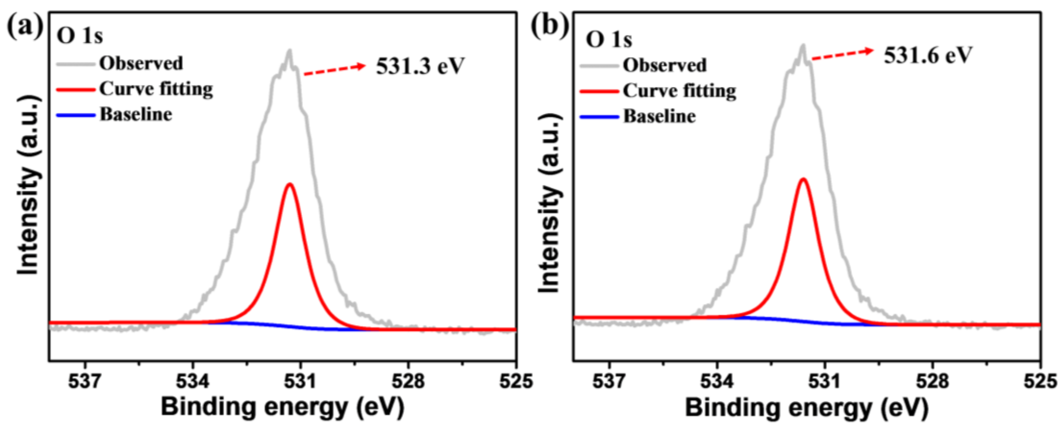

Figure S3. XPS spectra of O 1s in (a) natural wood and (b) Zr-wood.

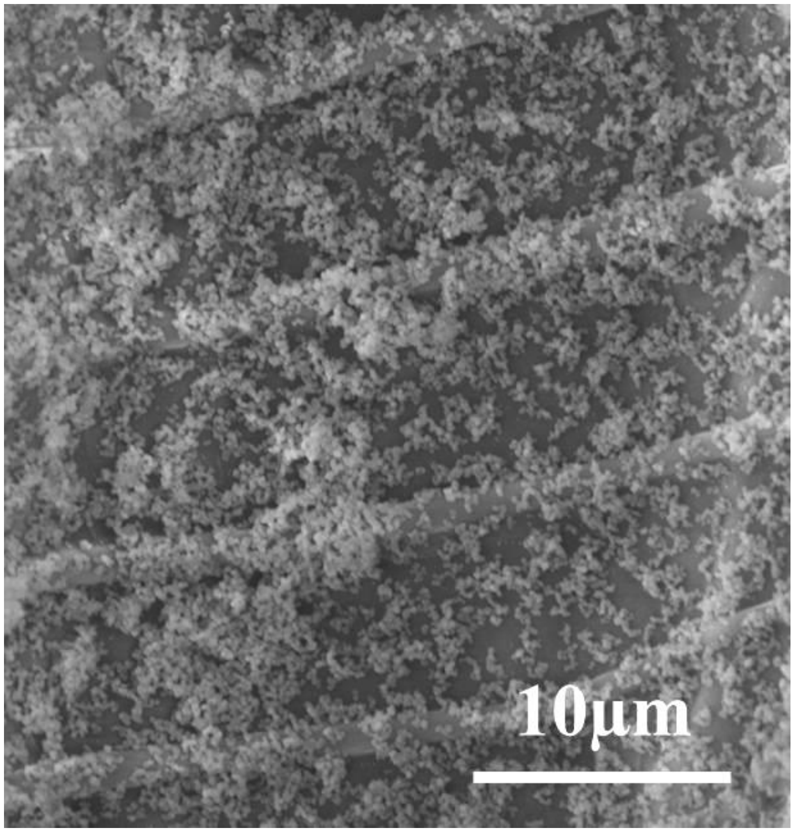

Figure S4. SEM image of UiO-66 MOFs nanoparticles in the microchannels of UiO-66/wood membrane.

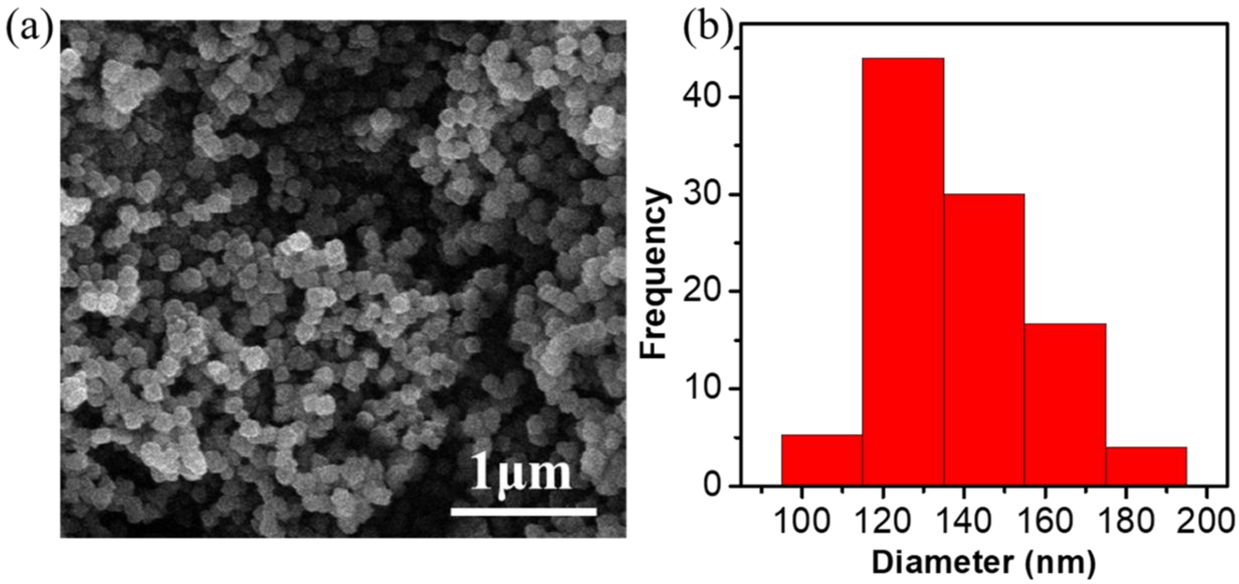

Figure S5. (a) SEM image of the UiO-66 MOFs nanoparticles in wood channels. (b) Size distribution of the UiO-66 MOFs nanoparticles. The average size of the UiO-66 MOFs nanoparticles is about 130 ± 10 nm.

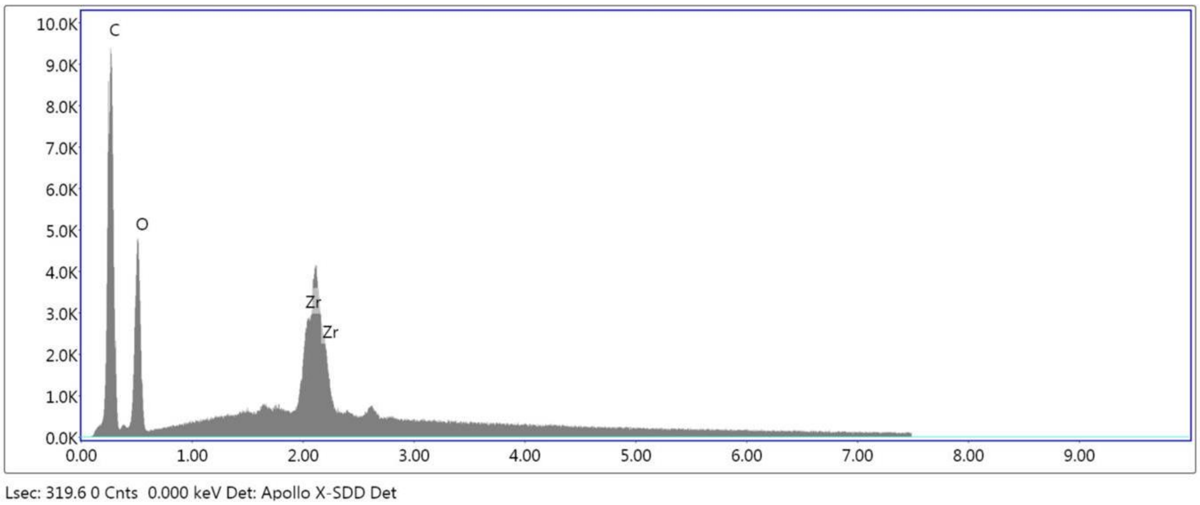

Figure S6. Energy dispersive X-ray spectroscopy (EDX) spectrum of the UiO-66/wood membrane.

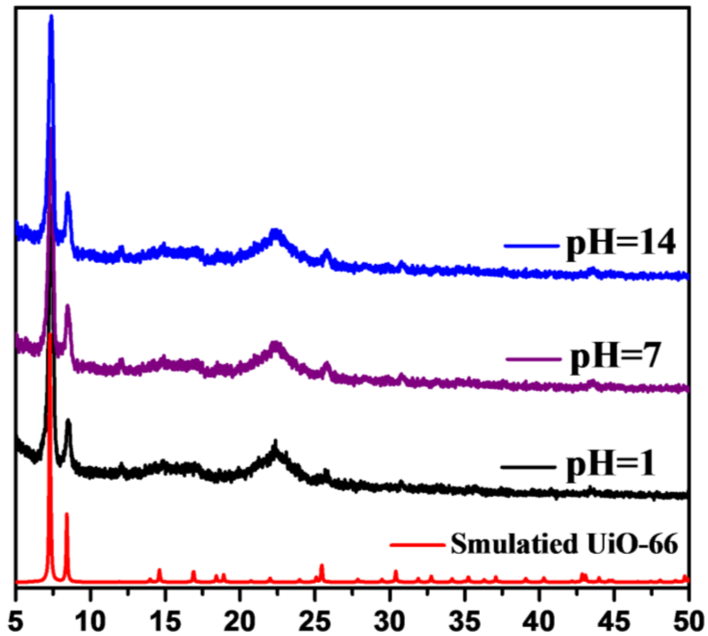

Figure S7. XRD patterns of UiO-66/wood composites showing the stability after immersed in solution with different pH values for 24 hours.

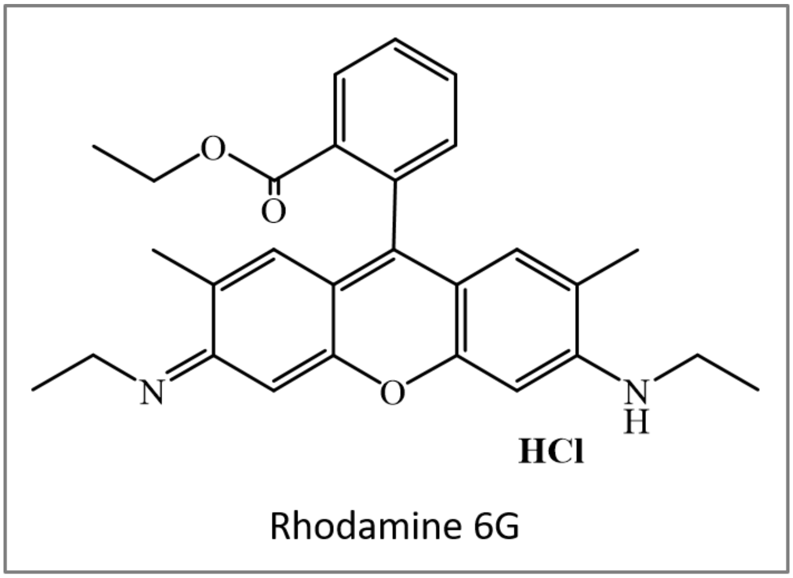

Figure S8. Molecular structure of Rh6G.

Contaminant Adsorption experiments

Rh6G sorption kinetics. The adsorption kinetic was performed at 25 °C. A piece of UiO-66/wood membrane (20 mg, UiO-66 MOFs: 2.22 wt %) was cut to chips and then added to a 100 mL beaker, which included 50 mL aqueous solution of Rh6G (10 $mg \cdot L^{-1}$). The mixture was shaken for 2 hours. The supernatant was taken out at different specific time periods and filtered. The concentration of Rh6G in filtrate was analyzed by UV-*vis* spectra (λ = 525 nm).

The distribution coefficient K_d is an important parameter to measure the performance of the adsorbents. The value of K_d can be determined by [39]

$$K_d = (C_i - C_f)/C_f \times (V/m) \qquad (1)$$

where C_i indicates the initial concentration of the contaminant ($mg \cdot L^{-1}$), C_f indicates the final equilibrium concentration of the contaminant ($mg \cdot L^{-1}$), m is the mass of the adsorbent (g), and V is the volume of the tested liquid (mL).

the adsorbed amount for Rh6G (q_t) was determined by the below equation.

$$q_t = (C_o - C_t)/m \times V \qquad (2)$$

where C_o and C_t are the concentration of the Rh6G ($mg \cdot L^{-1}$) initially and at time t, respectively, V is the volume solution used (L), and m is the mass of UiO-66 MOFs (g).

Mathematical Models. The adsorption kinetics of pseudo-first-order rate equation and pseudo-second-order rate equation was used to investigate the adsorption process. The adsorption kinetic equations are given as Eq 3 and Eq 4, respectively.[1,2]

$$\mathrm{Log}\,(q_e - q_t) = \log q_e - k_1 t \qquad (3)$$

$$t/q_t = 1/(k_2 q_e^2) + t/q_e \qquad (4)$$

where q_e and q_t are the amount of Rh6G adsorbed at equilibrium and time t (min), and k_1 (min^{-1}) and k_2 ($g \cdot mg^{-1} \cdot min^{-1}$) are the rate constant of the pseudo-first-order adsorption and the pseudo-second-order rate constant, respectively.

Rh6G adsorption isotherm. The adsorption isotherm of Langmuir and Freundlich models was used to further understand the adsorption mechanism. The adsorption isotherm equations are given as Eq 5 and Eq 6, respectively.[3,4]

$$C_e/q_e = 1/(k_L q_m) + C_e/q_m \quad (5)$$

$$\log q_e = \log K_f + (1/n)\log C_e \quad (6)$$

where q_e and q_m represent the equilibrium and the maximum adsorption capacity ($mg \cdot g^{-1}$), respectively. Here, C_e is the Rh6G concentration ($mg \cdot L^{-1}$) at equilibrium, and K_L ($L \cdot mg^{-1}$) is the Langmuir constant. Also, K_f ($L \cdot mg^{-1}$) and n are the Freundlich parameters related to adsorption capacity and adsorption intensity, respectively.

According to the above equations, conclusion can be drawn that:

(1) The K_d values of the UiO-66/wood membrane for Rh6G can reach 2.6×10^6 $mL \cdot g^{-1}$.

(2) The pseudo-second-order rate model and the Langmuir model were selected as the adsorption kinetic and the adsorption isotherm between Rh6G and UiO-66/wood composite.

(3) The adsorbed capacity of UiO-66/wood based on the content of UiO-66 MOFs for Rh6G is up to 690 $mg \cdot g^{-1}$.

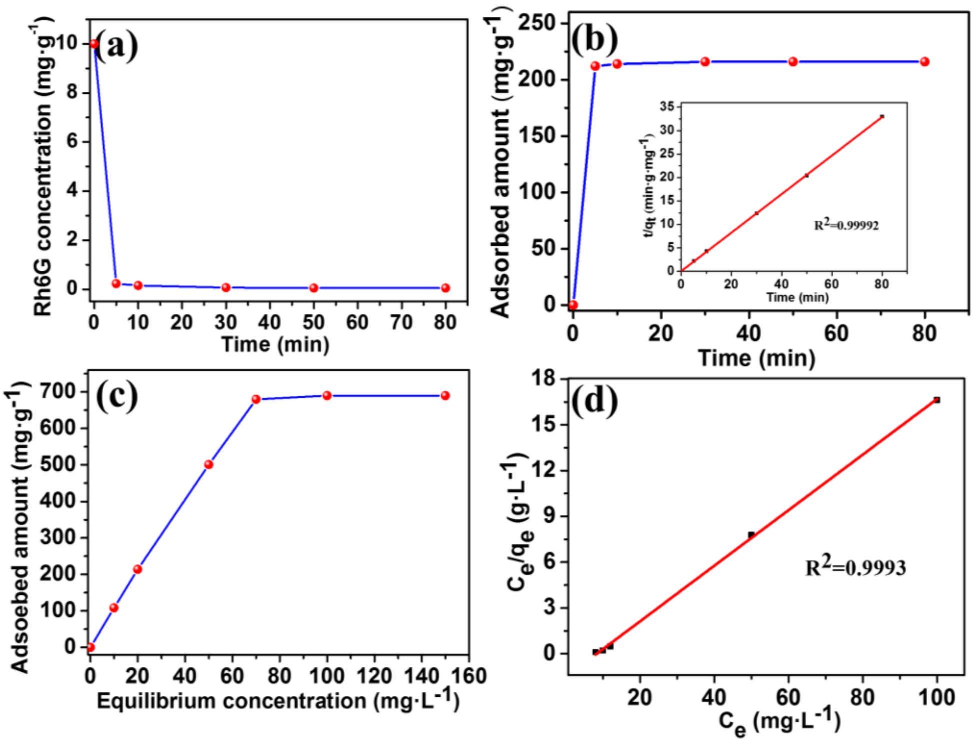

Figure S9. (a) The adsorption kinetic of UiO-66/wood composite for Rh6G at the initial concentration of 10 mg·L^{-1}. (b) Adsorption curve of Rh6G versus contact time using UiO-66/wood composite. Inset: Pseudo-second-order kinetic plot for Rh6G adsorption. (c) Adsorption isotherm of UiO-66/wood composite for Rh6G. (d) Linear regression by fitting the data with Langmuir adsorption model.

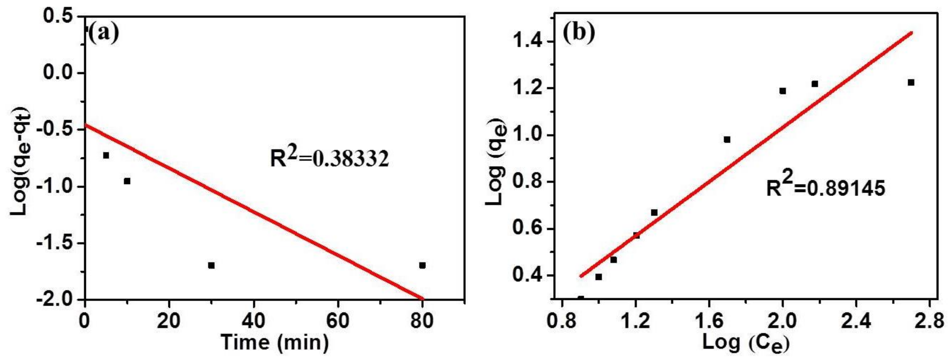

Figure S10. (a) Pseudo-first-order kinetic plot and (b) Freundlich isotherms for the adsorption mechanism between Rh6G and UiO-66/wood composite (Rh6G concentration: 10 mg·L^{-1}).

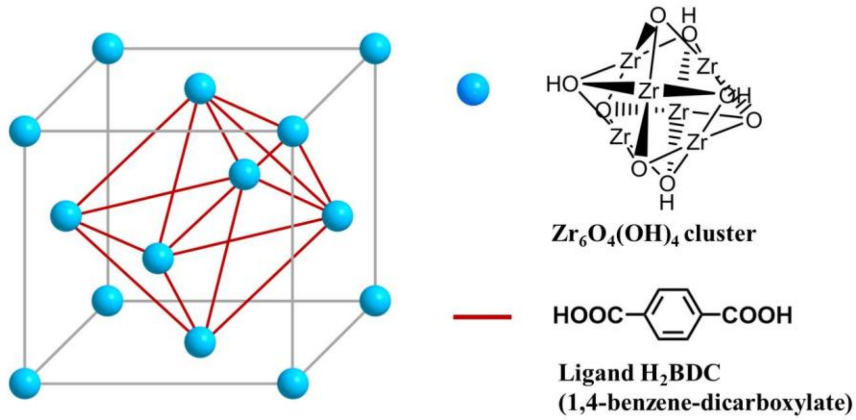

Figure S11. The structure of UiO-66 constructed with Zr_6 cluster and BDC ligand.

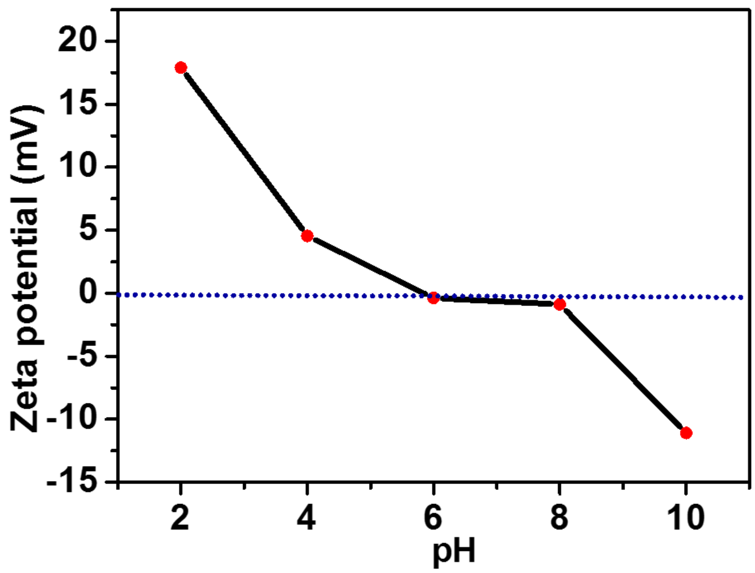

Figure S12. Zeta potential of UiO-66/wood composite in aqueous solution with different pH values.

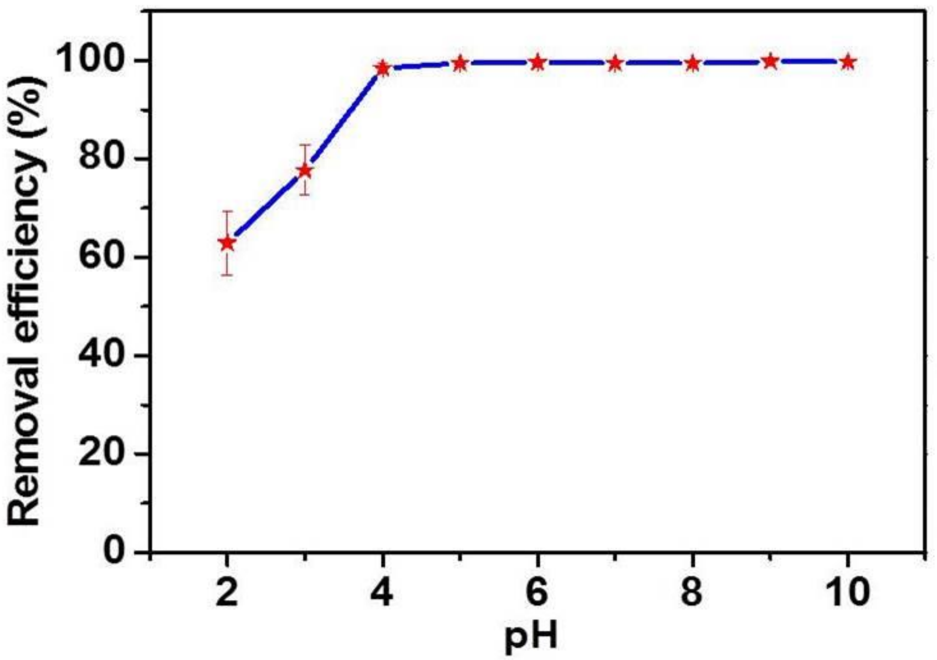

Figure S13. The removal efficiency of the three-layer filter (Flux: 1.0×10^{3} $L\cdot m^{-2}\cdot h^{-1}$) towards Rh6G (10 $mg\cdot L^{-1}$) at different pH values.

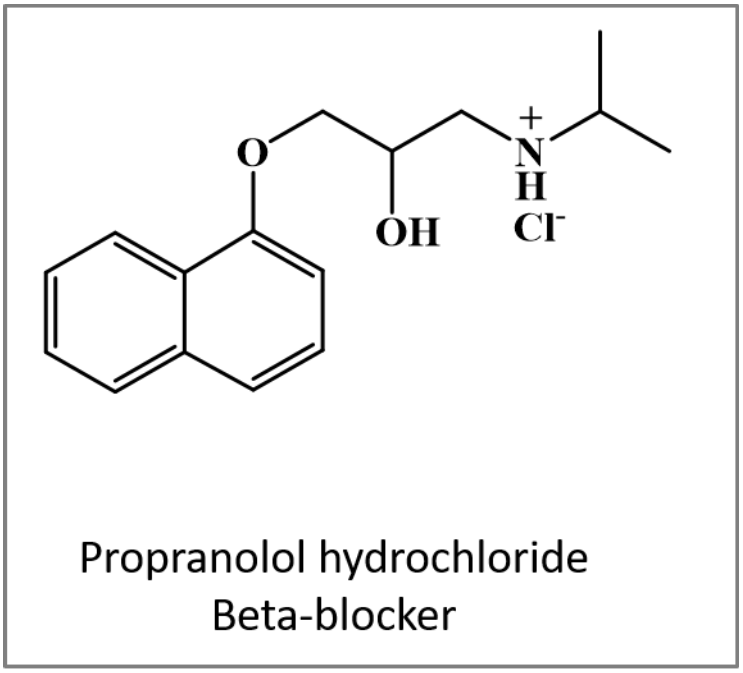

Figure S14. Molecular structure of the propranolol.

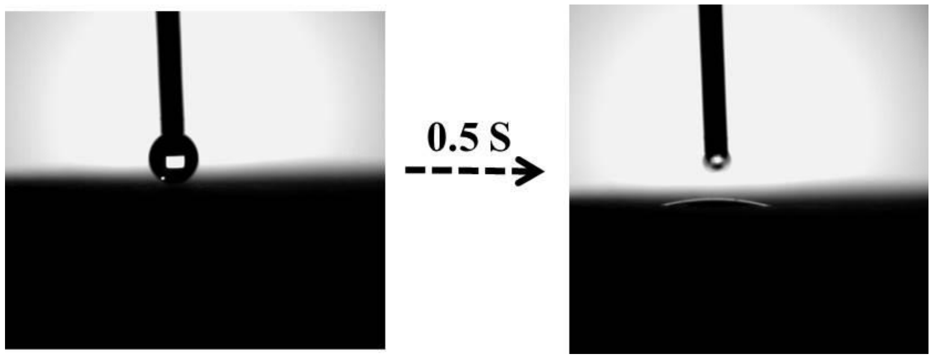

Figure S15. Water contact angle of UiO-66/wood membrane.

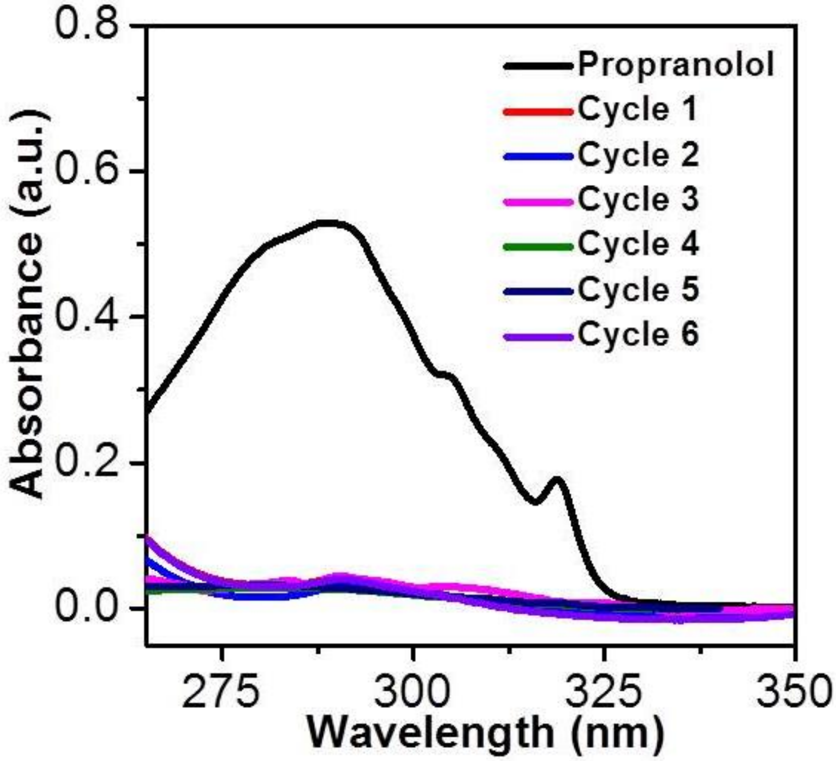

Figure S16. The UV-*vis* spectra of the propranolol solution before and after treated with the UiO-66/wood membrane for different cycles.

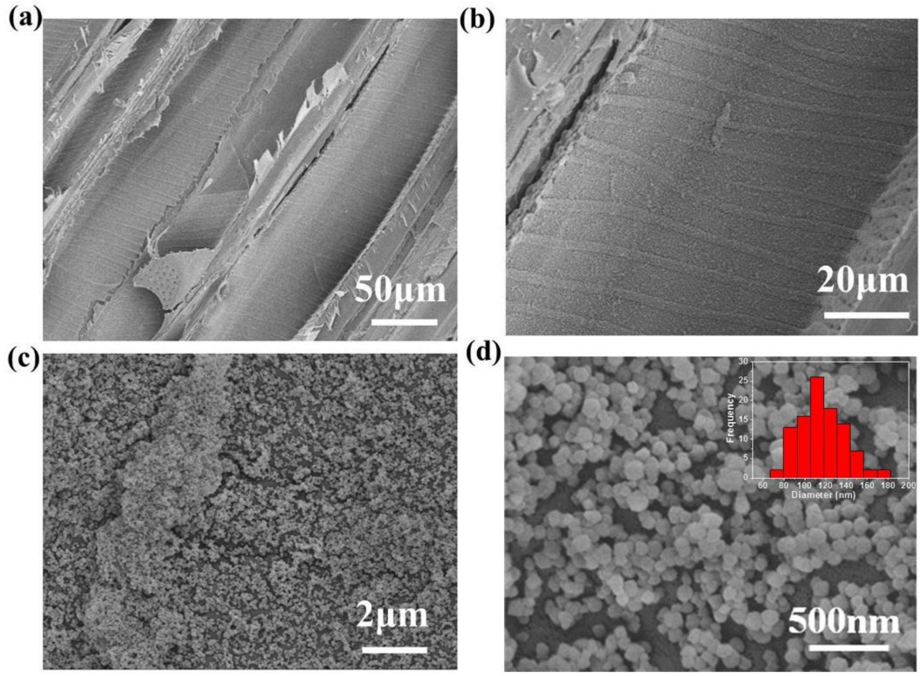

Figure S17. Different magnified SEM images of the UiO-66/wood membrane after 6 recycle. Inset shows the size distribution of UiO-66 MOFs after 6 recycle.

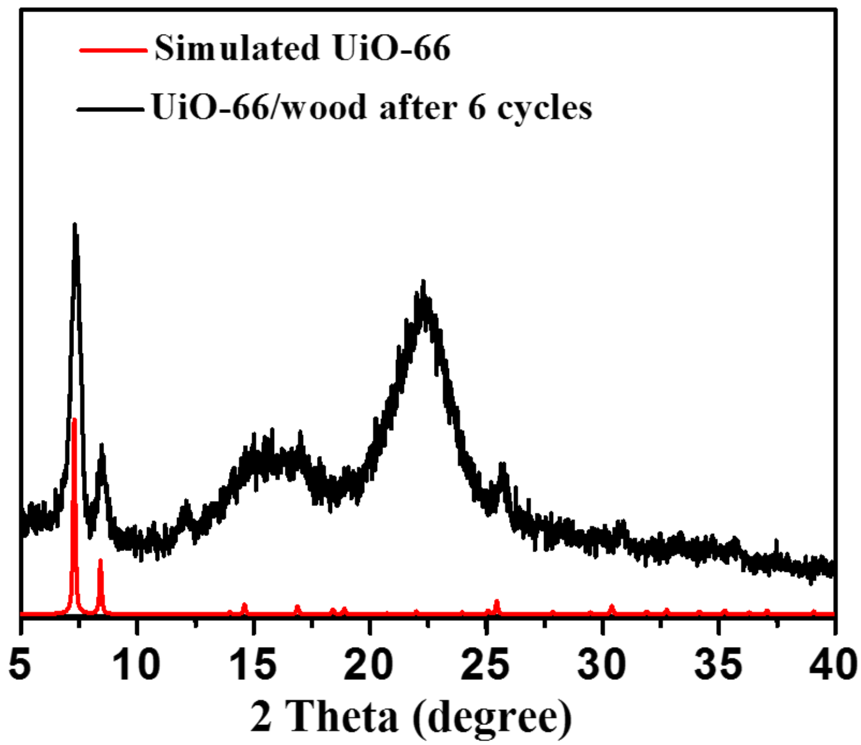

Figure S18. XRD patterns of simulated UiO-66 and UiO-66/wood membrane after 6 cycles.

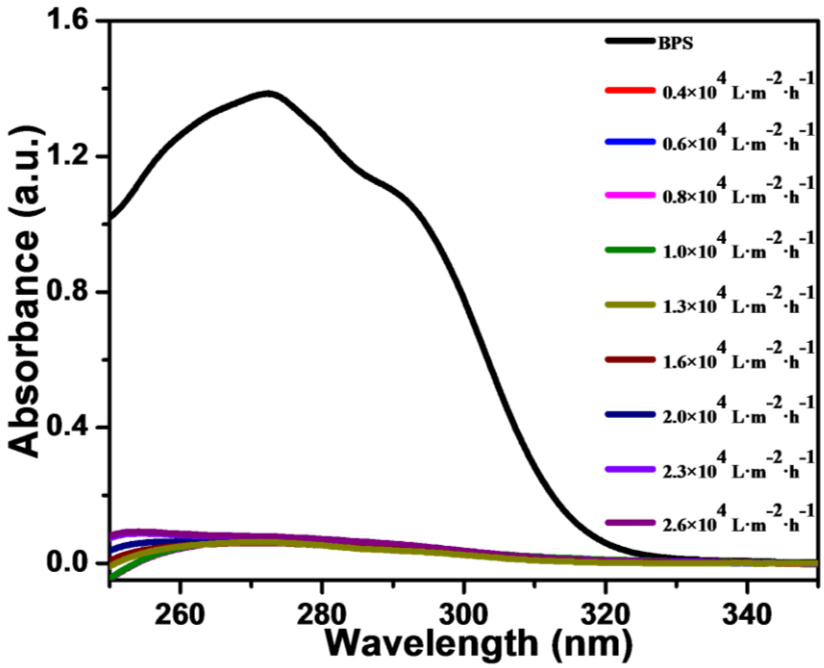

Figure S19. UV-*vis* spectra of the BPS solution (0.1 mmol·L^{-1}) before (in black) and after (in colors) the treatment using the UiO-66/wood membrane based three-layer filter at different flux rate.

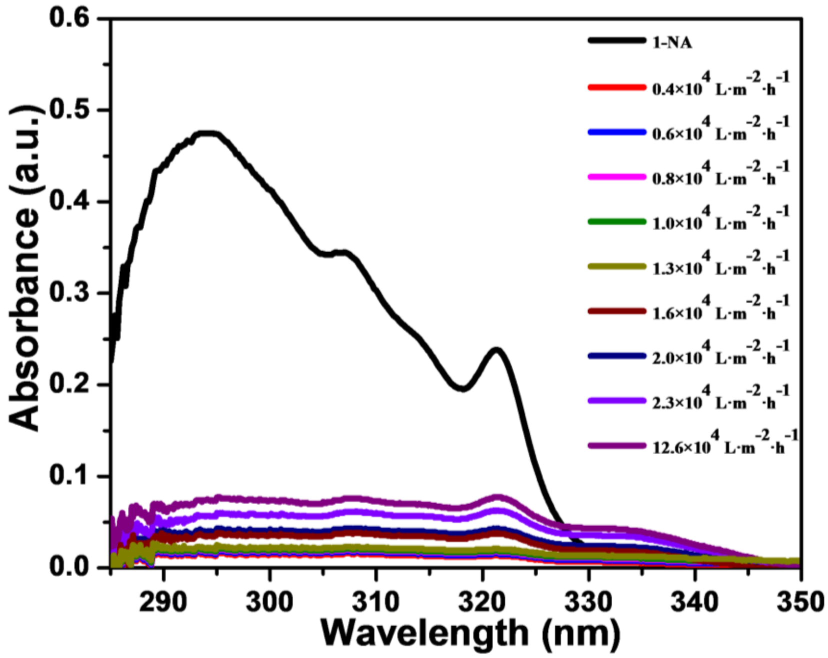

Figure S20. UV-*vis* spectra of the 1-NA solution (0.1 mmol·L^{-1}) before (in black) and after (in colors) treated using the UiO-66/wood membrane based three-layer filter at different flux rate.

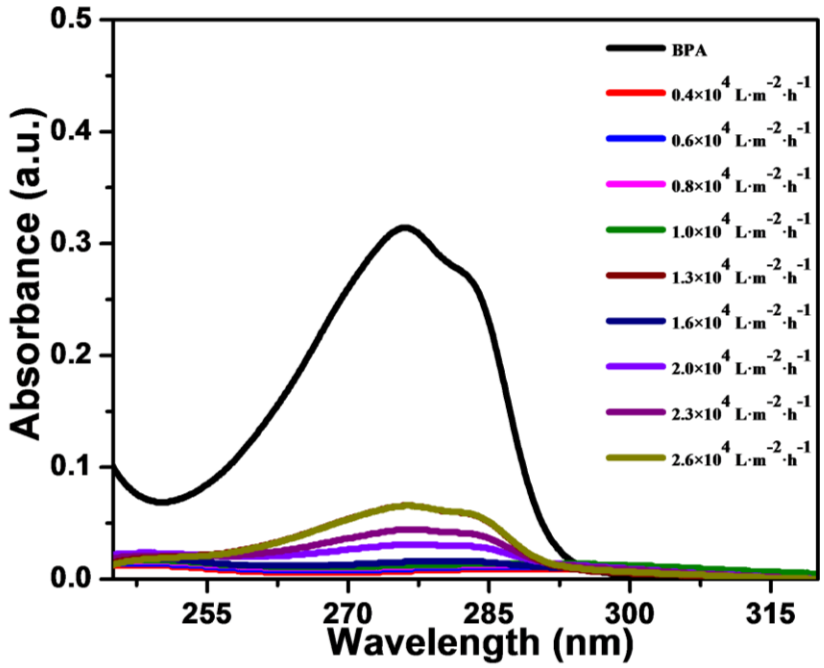

Figure S21. UV-*vis* spectra of the BPA solution (0.1 mmol·L^{-1}) before (in black) and after (in colors) the treatment using the UiO-66/wood membrane based three-layer filter at different flux rates.

Table S1. ICP analysis for the content of Zr and the calculated UiO-66 loading amount.

Molar mass of Zr ($g \cdot mol^{-1}$)	Molar mass of UiO-66 ($g \cdot mol^{-1}$)	Content of Zr (wt%)	Loading amount of UiO-66 (wt%)
91.2	1662.0	0.73	2.22

Table S2. The molecular size of various pollutants. [5]

Pollutant	molecular size (Å)
1-NA	16.3×9.5×5.8
BPA	12.5×7.9×6.7
BPS	12.5×7.2×6.7
Propranolol	16.2×9.4×6.0
Rhodamine 6G	16.7×12.5×11.4

The present molecular size was calculated with Gaussian 09w.

Table S3. Physical and chemical properties of the selected organic pollutants. [6]

Selected target	Rh6G	BPA	BPS	Propranolol	1-NA
molecular weight	479.01	228	250.27	259.01	143.19
solubility	Soluble in water	Slightly soluble in water	Soluble in water	Soluble in water	Slightly soluble in water
$logK_{ow}$	7.22550	3.4	3.01140	2.96840	3.00320
catogery	Dye	Endocrine disruptor	Endocrine disruptor	Beta-blocker	Carcinogen
toxicity in terms of LD_{50} ($mg{\cdot}Kg^{-1}$)	400	2000-5000	2830	9.334-9.450	779

Table S4. The organic pollutants removal efficiency of UiO-66/wood membrane compared to other materials reported in literature.

Materials	Pollutants	Removal efficiency (%)	Recycling	Reference
UiO-66/wood membrane	Rh6G	98	6	Our work
	BPA	98	6	
	BPS	98	6	
	1-NA	98	6	
	Propranolol	98	6	
B-ZnO nanoparticles	Rh6G	80.7	Not mentioned	Ref 57
Z9-600	Rh6G	91	4	Ref 54
CD-TFP@cotton	BPA	60	4	Ref 55
Fe_3O_4@SiO_2-PGMACD	BPA	89	5	Ref 56
P-CDP	BPA	95	5	Ref 58
	BPS	85	5	
	1-NA	92	5	
	Propranolol	96	5	

Reference

(1) Ho, Y. S. Citation review of Lagergren kinetic rate equation on adsorption reactions. *Scientometrics.* **2004**, 59 (1), 171-177.

(2) Ho, Y. S.; Ng, J. C. Y.; McKay, G. Kinetics of pollutant sorption by biosorbents: review. *Sep. Purif. Rev.* **2000**, 29 (2), 189-232.

(3) Langmuir, B. I. The Constitution and fundamental properties of solids and liquids. *J. Am. Chem. Soc.* **1916**, 38 (11), 2221-2295.

(4) Andjelkovic, I.; Tran, D. N. H.; Kabiri, S.; et al. Graphene aerogels decorated with α-FeOOH nanoparticles for efficient adsorption of arsenic from contaminated waters. *ACS Appl. Mater. Interfaces.* **2015**, 7 (18), 9758-9766.

(5) Gaussian 09, Revision B.01: Frisch, M. J. et al. Gaussian, Inc.: Wallingford, CT, **2009**.

(6) https://www.wikipedia.org/?tdsourcetag=s_pctim_aiomsg